

Correlation of electronic structure and martensitic transition in epitaxial Ni₂MnGa films

G. Jakob, T. Eichhorn, M. Kallmayer, and H. J. Elmers

Institut für Physik, Universität Mainz, Staudinger Weg 7, D-55099 Mainz, Germany

(Received 22 August 2007; revised manuscript received 9 October 2007; published 2 November 2007)

We investigate the martensitic transition of single crystalline Ni₂MnGa(110)/Al₂O₃(11 $\bar{2}$ 0) and Ni₂MnGa(100)/MgO(100) films using magnetometry, x-ray diffraction, x-ray absorption spectroscopy, and x-ray magnetic circular dichroism. The martensitic transition from the cubic austenite phase to the low symmetry martensite phase depends strongly on the chosen substrate. For (110) oriented films on Al₂O₃, the martensitic phase is significantly more stable than for the (100) oriented films on MgO. A remarkable change of the Ni x-ray absorption spectra occurs at the transition, indicating specific changes of the electronic structure. The observed changes are in agreement with theoretical predictions. The orbital to spin momentum ratio of the Ni moment increases significantly on entering the martensite state, thus explaining the macroscopic increase of magnetic anisotropy.

DOI: 10.1103/PhysRevB.76.174407

PACS number(s): 75.30.Gw, 81.30.Kf, 71.20.Lp, 78.70.Dm

I. INTRODUCTION

Martensitic phase transitions are displacive first order transitions from cubic high temperature phases (austenite) to tetragonally distorted low temperature phases (martensite). Due to their technological importance, they have a long history of scientific interest. Ni₂MnGa is an especially interesting martensite structure, as it is a magnetic shape memory material.¹ It can change its macroscopic shape under application of an external magnetic field. Due to an exceptionally large c/a ratio of the tetragonal distortion, large length changes up to 10% can be achieved in single crystals.^{2,3}

Ni₂MnGa is at room temperature in a cubic ferromagnetic Heusler phase, which shows order of the $L2_1$ type. The latter is characterized by four interpenetrating single atom type fcc lattices, where the base atoms are located at, e.g., Ga (0,0,0), Mn (0, 1/2, 0), and Ni (1/4, 1/4, 1/4) and (3/4, 1/4, 1/4) (see right inset of Fig. 1). The cubic $L2_1$ structure changes at the martensite transition (MST) to the low temperature martensite (MS) phase,⁴ which is to first approximation a tetragonal phase, where the c axis of the martensite is shrunk with respect to the austenite (AS). Often the a and b axes undergo compensating changes, keeping the unit cell volume constant. X-ray diffraction, neutron diffraction, and transmission electron microscopy showed that additional periodic distortions of successive (110) atomic planes can lead to fivefold and sevenfold superstructures.⁵⁻⁷ Details of the structure are very sensitive to the preparation conditions. Also, the transition temperature strongly depends on the exact sample stoichiometry.⁸

On the microscopic level, few results with respect to magnetism and electronic structure are established. While Zayak *et al.*⁹ found a global energy minimum of the martensitic phase for a ratio $c/a > 1$, a stable martensitic phase at $c/a = 0.97$ was reported by Barman *et al.*¹⁰ Nevertheless the *ab initio* calculations indicate an electronic instability as the cause for the MST.⁹⁻¹¹ The change of the electronic structure at the phase transition mostly involves Ni-derived minority d states. States with Ni $3d_{z^2}$ and $3d_{x^2-y^2}$ symmetries, which are degenerated in the cubic state, split up in the tetragonal phase. An abrupt decrease of the Ni moment (m_{Ni}) is calcu-

lated, while the Mn moment m_{Mn} remains constant at the MST.¹⁰ According to the comparatively large structural change, Ayuela *et al.*¹¹ predicted that the band structure modification at the MST should lead to experimentally observable changes of the band structure, as, e.g., in energy dependent x-ray absorption (XAS) spectra. In contrast to metal-insulator transitions, changes at the MST in Ni₂MnGa are more subtle, as the transition is between two different ferromagnetic metallic phases. In spite of the generality of martensite transitions, we are not aware of an experimental test of theoretically predicted band structure changes at the MST.

For XAS spectroscopy, we exploit the x-ray luminescence of the substrates in order to directly measure the change of the electronic structure at the MST of Ni₂MnGa confirming previous theoretical predictions.¹¹ Briefly, we prepared single crystalline Ni₂MnGa films and identified the MST by x-ray diffraction (XRD) and magnetometry. The Ni-XAS spectra

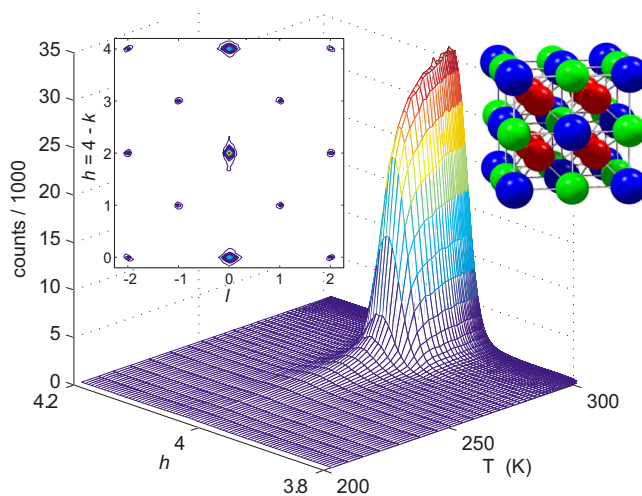


FIG. 1. (Color online) 3D plot of $(h00)$ scans of the (400) XRD reflection of the AS phase, indicating the MST with decreasing temperature. The individual scans were taken at constant temperature. The right inset shows the austenite phase. The left inset displays the twofold symmetry of the scattered intensity.

reveal a distinct variation at the MST in agreement with theory, which is the central result of this work. Besides the drop of m_{Ni} at the MST, ground-state calculations for the related Heusler compound NiMnSb suggest a much stronger temperature dependence for m_{Ni} compared to m_{Mn} .¹² Contrarily, neutron scattering showed a steady m_{Ni} but decreasing m_{Mn} for NiMnSb.¹³ In order to test the theoretical predictions, we have applied x-ray magnetic circular dichroism (XMCD) as an ideal tool for the independent determination of Mn and Ni moments.

II. EXPERIMENT

We have grown Ni₂MnGa films by dc-magnetron sputtering onto Al₂O₃(11 $\bar{2}$ 0) and MgO(100) substrates at 500 °C. The sputtering system has a base pressure of 3×10^{-8} mbar and is equipped with homemade sputtering guns. Before and during deposition of the Heusler compound, we have a titanium cathode sputtering onto a liquid nitrogen cooled cold trap containing the gas inlet, in order to minimize water and oxygen partial pressure. The 50 mm diameter target was cut by spark erosion from melt cast pieces of the stoichiometric compound produced by the Institut für Werkstofforschung, Dresden. Typical deposition parameters are 0.05 mbar argon pressure and 100 mA current at 320 V voltage, resulting in a deposition rate of 1.3 nm/s at a substrate distance of 30 mm. The sputtering system has been used for different types of Heusler thin films.^{14,15} Here, we investigated films with a typical thickness of 100 nm.

Magnetic measurements were performed using a superconducting quantum interference device and a vibrating-sample magnetometer. For temperature dependent x-ray diffraction, we used a four circle rotating anode system equipped with a He-gas cryostat that allows direct mapping of scattered intensity in reciprocal space coordinates.

The XAS experiments were performed at the UE56/1-SGM beamline at the German synchrotron light source BESSY II (Berlin). The incident photon flux was monitored by a Au net. The total electron yield was measured via the sample current. In order to collect all electrons, the sample was shielded by a conducting tube on a positive bias voltage (100 V). For the XAS signal, the photon flux transmitted through the thin film was detected via x-ray luminescence in the substrate. The luminescence light intensity was measured by a GaAs photodiode. The GaAs photodiode was protected by a transparent cap layer in order to prevent detection of x-ray fluorescence light from the sample surface. An external magnetic field of 1.6 T saturates the sample magnetization perpendicular to the film surface. We kept the x-ray polarization constant and flipped the magnetic field to determine the XMCD signal. More details are reported elsewhere.¹⁶ The luminescence signal is much larger for Al₂O₃ than for MgO substrates. Therefore, we focus in the following on the films on Al₂O₃.

III. STRUCTURAL PROPERTIES

The XRD patterns of the thin films at room temperature in the cubic AS phase show a (110) orientation on Al₂O₃(11 $\bar{2}$ 0)

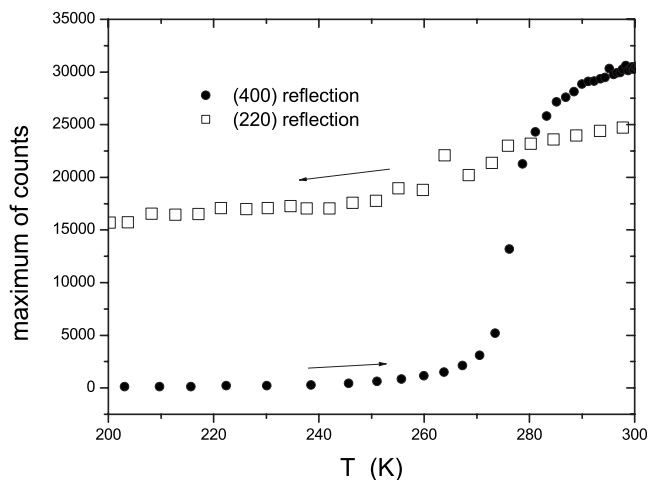


FIG. 2. Maximum count rate of the austenite (220) and (400) reflections as function of temperature.

substrates, while they are (100) oriented on MgO(100). The single crystalline nature of the thin film on Al₂O₃ is evident in the left inset of Fig. 1. It shows a contour plot of the intensity in a scattering plane perpendicular to the specular (220) reflection measured at room temperature. Clearly visible is the twofold symmetry and the presence of $L2_1$ -ordering reflections with all odd indices. The film in-plane [001] direction is parallel to the substrate [1 $\bar{1}$ 00] direction.¹⁴ This orientation is 90° rotated to the orientation expected from lattice constants mismatch but in agreement with results on other Heusler compounds.¹⁸ The main part of Fig. 1 displays ($h00$) scans of the (400) reflection of the austenite structure, which is a nonspecular reflection on Al₂O₃(11 $\bar{2}$ 0) substrate. In these scans, at constant temperature, the lattice constant along the respective direction of the reciprocal lattice is varied, while the direction of the scattering vector is fixed. Such that they correspond to usual $\theta/2\theta$ scans of this film reflection. At $T=276$ K, the intensity of the (400) peak of the original cubic austenite phase appears, indicating the martensite to austenite transition. The temperature dependence of the structural transition is shown in detail in Fig. 2. Remarkably, Ni₂MnGa(100) films on MgO(100) sputtered in the same run show the transition at $T=220$ K close to the bulk value. Therefore, the structural transition seems to be shifted to higher temperatures due to the film-substrate interaction. We think that this is not due to the epitaxial strain during growth, as the lattice constants in the cubic phase are identical in both cases ($a_{\text{cub}}=0.5822$ nm). However, the martensite transition requires the formation of (110) twin planes. For (100) oriented films on MgO, all possible twin planes will hit the substrate surface. The splitting of the cubic (400) reflection due to the formation of eight tetragonal martensite variants is evident in Fig. 3 for a film on MgO (100), which possesses a fourfold symmetry of the substrate surface. Part (a) [(b)] of this figure shows the four equivalent variants, where the longer a axis (shorter c axis) is nearly perpendicular to the film plane. Assignment of a axis and c axis is based on volume conservation during the transition. Two variants connected by a common twinning

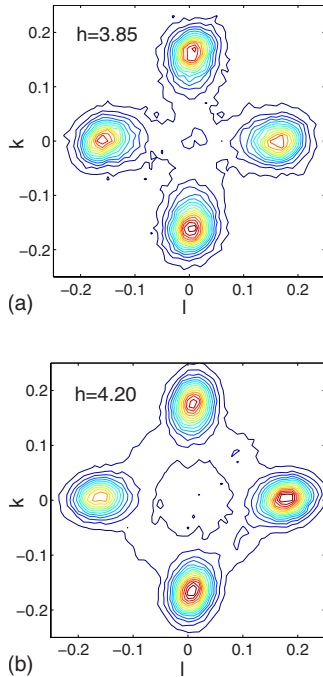


FIG. 3. (Color online) Contour plot of kl scans near the original, specular (400) XRD reflection of the AS phase. In the martensite phase, intensity is detected at the reciprocal lattice plane with coordinates $(h=3.85 k l)$ (a) and $(h=4.20 k l)$ (b), respectively.

plane enclose an angle of 4.7° and cause opposing reflections, e.g., the top reflection in Fig. 3(a) and the bottom reflection in Fig. 3(b).

Only for the (110) oriented films on $\text{Al}_2\text{O}_3(11\bar{2}0)$, twin planes parallel to the substrate surface are possible. A detailed study of the full twinning structure could not be performed on $\text{Al}_2\text{O}_3(11\bar{2}0)$ due to the geometrical limits of the cryostat setup (not all symmetry equivalent reflections are accessible). Nevertheless, the twinning structure explains the different behavior of the austenite (400) and (220) reflections in Fig. 2. The tetragonal (202) reflection²¹ contains components from both a and c axes. The changes associated with the MST seem to compensate in our sample. From our four circle measurements on films on MgO, we find $c/a=0.92$ with $a_{tet}=1.038a_{cub}$ and $c_{tet}=0.9516a_{cub}$. Thus, the lattice plane distances are nearly identical $d_{202,tet}/d_{220,cub}=0.992$. As for the films on Al_2O_3 no significant shift of the austenite (220) reflection is observed, we conclude that the tetragonal distortion is similar to films on MgO. The tetragonal (400) reflection, however, shows no compensation. The fact that we do not observe a peak intensity for this reflection in the longitudinal scan shown in Fig. 1 below the phase transition requires that its direction also changes during the phase transition due to twinning. We can observe it at low temperatures for one of the martensite variants, e.g., at $(h k l) = (3.80 0.21 0.08)$ using cubic reciprocal space coordinates.

IV. MAGNETIC PROPERTIES

Measurements of the temperature dependent magnetization reveal a Curie temperature $T_C=360$ K of our thin film

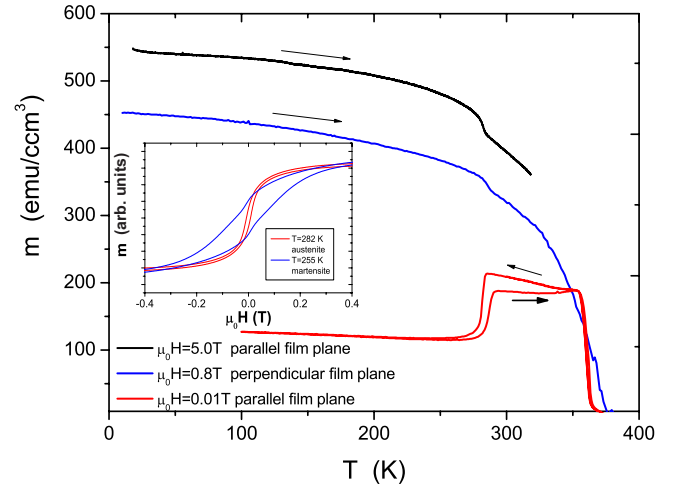


FIG. 4. (Color online) Magnetization vs temperature for a Ni_2MnGa film on Al_2O_3 substrate. The high field data have been corrected with a constant diamagnetic contribution from the substrate. Inset: hysteresis loops for film parallel magnetic field at temperatures above and below the MST.

samples independent of the chosen substrate. The MST shows up in small field magnetization measurements with field applied parallel to the film plane as a sharp drop of the magnetization, indicating a change of the easy axis direction. In Fig. 4, arrows mark the direction of temperature variation and a clear hysteresis of 7 K width of the phase transition is observed. Hysteresis loops show the coercive field to increase from 8 to 50 mT when entering the martensite state. Measurements in high fields reveal an increase of the total magnetic moment at the martensite transition in accordance with observations on the bulk material⁷ and theoretical calculations.¹¹ Typical values of the saturation magnetization are $\sim 3 \mu_B/\text{f.u.}$, which is lower than that of $4.2 \mu_B/\text{f.u.}$ reported for bulk samples. We attribute this discrepancy to an atomic disorder which leads to deviations from the perfect $L2_1$ order. The general magnetization behavior for our films is in agreement with that expected for bulk Ni_2MnGa .

In order to obtain element-specific information on the electronic structure, we measured the XAS and XMCD at the Mn and Ni $L_{2,3}$ edges in the transmission mode¹⁷ for various temperatures below and above T_{MST} . Figures 5 and 6 show data calculated from the incident-photon-flux-normalized transmission XAS spectra of a $\text{Ni}_2\text{MnGa}(110)/\text{Al}_2\text{O}_3(11\bar{2}0)$ Heusler alloy film at temperatures below and above the martensitic phase transition for Mn and Ni, respectively. Assuming that the luminescence signal of the substrate $I^\pm(h\nu)$ is proportional to the transmitted x-ray intensity, the x-ray absorption coefficient k is given by $k^\pm(h\nu) = \mu^\pm(h\nu)d = -\ln[I^\pm(h\nu)/I_{ref}(h\nu)]$ [Figs. 5(a) and 6(a)]. The reference spectra $I_{ref}(h\nu)$ increase linearly with the photon energy. The absolute value of $I_{ref}(h\nu)$ was then normalized at the preedge region of the corresponding element. The slope of the reference spectra was adjusted to get the same absorption step height in all cases. The resulting x-ray absorption coefficient reflects the unoccupied local density of states function (LDOS). Figures 5(b) and 6(b) show the corresponding

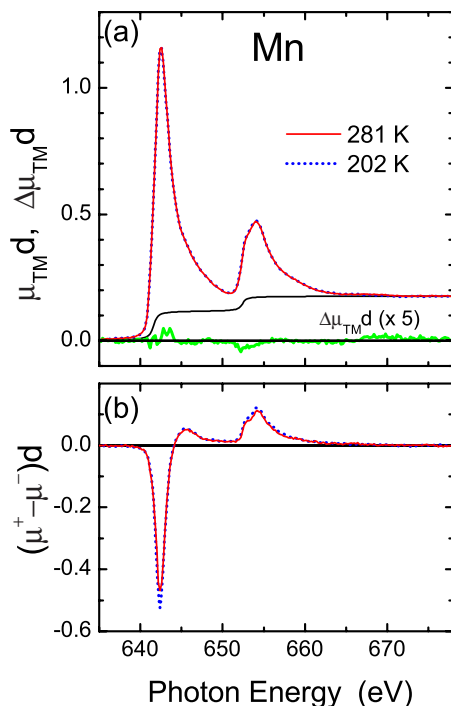


FIG. 5. (Color online) (a) Absorption coefficient $k=(k^++k^-)/2 = \mu_{\text{Mn}}d = -\ln(I/I_{\text{ref}})$ of x-ray light transmitted through a $d=83$ nm thick Ni_2MnGa (110) film on $\text{Al}_2\text{O}_3(11\bar{2}0)$ at the Mn L_3 edge for $T < T_{\text{MST}}$ (dashed blue line) and $T > T_{\text{MST}}$ (full red line). The green line is the difference curve $\Delta\mu_{\text{Mn}}d$ multiplied by a factor of 5. (b) XMCD signal $(\mu^+ - \mu^-)d$ for the respective temperatures.

XMCD signals for the elements Mn and Ni calculated from the respective spectra measured with opposite magnetization direction.

We find a clear change of the intensity of feature A in the Ni L_3 absorption signal [indicated in Figs. 6(a) and 7(a)] at T_{MST} . This peak is well pronounced in the cubic phase above T_{MST} and it is nearly suppressed in the tetragonally distorted phase below T_{MST} . A similar change of the spectrum also occurs at the L_2 edge, however, with a larger lifetime broadening. The lifetime of the $2p_{1/2}$ core hole is much shorter than the $2p_{3/2}$ core hole due to the Coster-Kronig decay. Therefore, we focus on the discussion of the L_3 energy region. For better comparison to theory, we replot this part of the spectra in Fig. 7.

V. DISCUSSION

The observed increase of feature A at the phase transition is in full agreement with the theoretical prediction by Ayuela *et al.*¹¹ [see Fig. 7(a)]. According to their calculations, the peak originates from hybridized Ni $3d$ -Ga $2p$ states that are degenerated in the austenite state. Their degeneracy is lifted by the martensitic transition leading to a reduction of the density of states at the respective energy position. The difference of the Ni spectra above and below T_{MST} reveals a second characteristic change with the opposite sign close to the Fermi edge. This is caused by a Ni $3d$ state of d_{z^2} character just above the Fermi edge. For $c/a < 1$, the correspond-

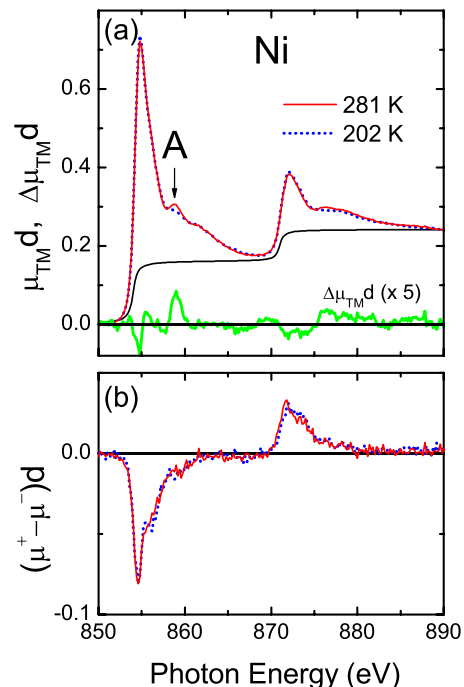


FIG. 6. (Color online) (a) Absorption coefficient $k=(k^++k^-)/2 = \mu_{\text{Ni}}d = -\ln(I/I_{\text{ref}})$ of x-ray light transmitted through a $d=83$ nm thick Ni_2MnGa (110) film on $\text{Al}_2\text{O}_3(11\bar{2}0)$ at the Ni L_3 edge for $T < T_{\text{MST}}$ (dashed blue line) and $T > T_{\text{MST}}$ (full red line). The green line is the difference curve $\Delta\mu_{\text{Ni}}d$ multiplied by a factor of 5. (b) XMCD signal $(\mu^+ - \mu^-)d$ for the respective temperatures.

ing peak in the Ni minority LDOS is narrowed in the martensitic phase with respect to the cubic structure, thus leading to the observed increase for $T < T_{\text{MST}}$.¹¹ The intensity of peak A shows a sharp increase at T_{MST} [Fig. 7(c)], confirming that the observed changes in the XAS spectra are related to the martensitic phase transition.

Changes at T_{MST} in the Mn $L_{3,2}$ spectra are hardly measurable. This is expected in the case of $c/a < 1$ where the Fermi level lies in a position at which there is almost an equal LDOS of majority and minority t_{2g} states. In the case of $c/a > 1$, larger changes of the LDOS would be caused by hybridization because the atoms become closer in the ab plane.¹¹ Thus, our observation indicates a structural change toward $c/a < 1$.

Spin and orbital magnetic moments resulting from a sum rule analysis^{19,20} of XMCD spectra are shown in Fig. 8. The Mn orbital moment is almost zero. Therefore, the magnetic anisotropy is exclusively caused by Ni. The orbital to spin moment ratio for Ni amounts to $\mu_{\text{orb}}/\mu_{\text{spin}}=0.15$ in the MS phase and decreases to 0.05 in the AS phase [Fig. 8(a)], passing a maximum of 0.18 in the transition region. An increased Ni orbital moment is indicative for a lower local symmetry of the corresponding crystal field. This is consistent with the lowest value measured in the AS phase with cubic symmetry. The lowest symmetry occurs in the transition region where Ni atoms show the largest position variations. An increased orbital moment in the MS state infers an increased local magnetic anisotropy. A large magnetic anisotropy is essential for the occurrence of the magnetic shape memory effect.

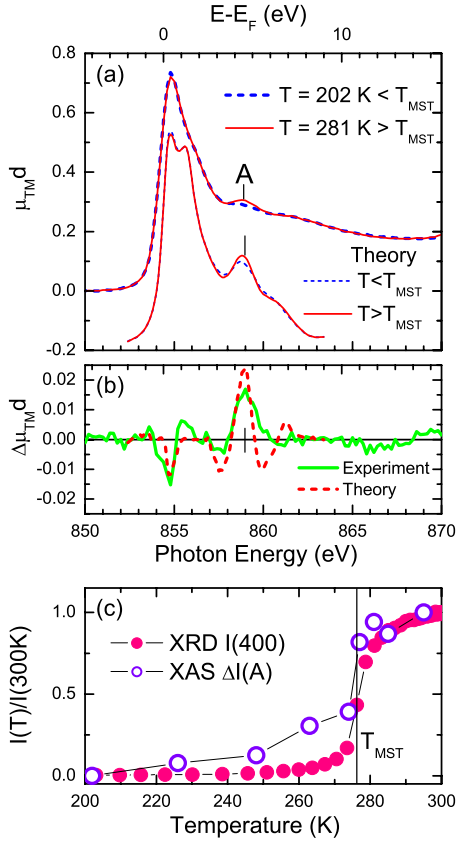


FIG. 7. (Color online) (a) Absorption coefficient for $T < T_{MST}$ (dashed blue line) and $T > T_{MST}$ (full red line). Corresponding data from *ab initio* theory (Ref. 11) are shifted for comparison. (b) Difference between the data shown in (a) for $T > T_{MST}$ and $T < T_{MST}$. (c) Temperature dependence of the intensity of the XRD (400) reflection (full circles, red), $I(400)$, and of the intensity increase $\Delta I(A) = I(T) - I(202 \text{ K})$ of feature A, as indicated in (a), in the Ni-XAS spectra (open circles), normalized to their respective room temperature values.

The Ni spin moment per empty d -electron state stays almost constant in the range 200–280 K at $\mu_{spin}/N_h = 0.17 \mu_B$. For Mn, we observe a decrease of the spin moment from $\mu_{spin}/N_h = 0.355 \mu_B$ at low temperature to $\mu_{spin}/N_h = 0.302 \mu_B$ at 295 K [Fig. 8(b)]. A stronger temperature dependence of m_{Mn} was also observed by neutron diffraction.¹³ We attribute the stronger temperature dependence of m_{Mn} to thermal fluctuations that are not explicitly considered by ground-state theories.

Considering the different values for N_h for Ni (1.3) and Mn (4.3) and also a correction factor for Mn of 1.5 because of the jj mixing, the ratio between Mn and Ni moments is roughly a factor of 10, in agreement with *ab initio* theory.^{10,11} However, we could not confirm the predicted drop of the Ni moment at T_{MST} . The saturation magnetization shows a decrease at T_{MST} [see Fig. 8(c)] in accordance with the bulk material⁷ and theoretical calculations.¹¹ The extrapolated saturation magnetization from XMCD at $T=0 \text{ K}$ is $3 \mu_B/\text{f.u.}$ in agreement with magnetometer measurements. Though the luminescence yield on MgO substrates is much lower, the evaluation of the data for $\text{Ni}_2\text{MnGa}(100)/\text{MgO}(100)$ films is

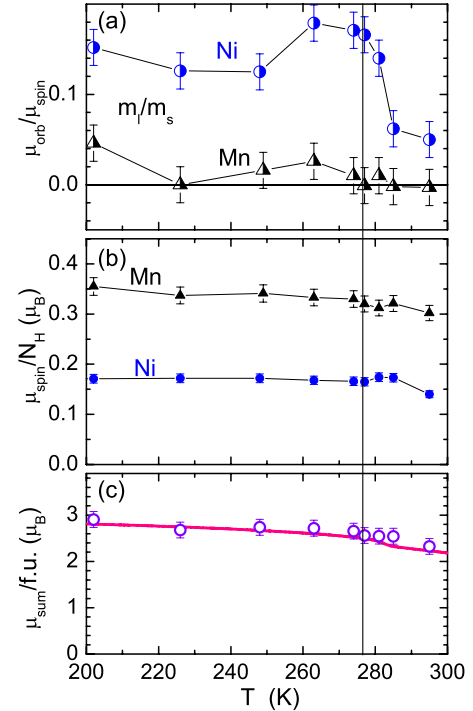


FIG. 8. (Color online) (a) Orbital to spin momentum ratio for Mn (black triangles) and Ni (blue circles) of the sample shown in Fig. 7. (b) Effective spin moments per d hole, N_h , for Mn (black triangles) and Ni (blue circles), excluding a jj -mixing correction factor (c_{jj}) in the case of Mn. (c) Sum moment per f.u. calculated from spin and orbital moments of Ni and Mn assuming $N_h(\text{Ni})=1.3$, $N_h(\text{Mn})=4.3$, and $c_{jj}=1.5$ (circles). Error bars denote the statistical error, only, not considering systematic errors due N_h , c_{jj} , and finite polarization. The full red line indicates saturation magnetization data measured by magnetometry (5 T). The vertical lines indicate T_{MST} .

qualitatively in full agreement with the results for $\text{Ni}_2\text{MnGa}(110)/\text{Al}_2\text{O}_3(11\bar{2}0)$.

VI. SUMMARY AND CONCLUSION

In summary, we investigated structural and electronic properties of $\text{Ni}_2\text{MnGa}(110)/\text{Al}_2\text{O}_3(11\bar{2}0)$ and $\text{Ni}_2\text{MnGa}(100)/\text{MgO}(100)$ shape memory alloy films at the martensitic phase transition. The temperature of the martensitic phase transition differs considerably between films grown on the two different substrates. The phase transition was investigated by temperature dependent x-ray diffraction, magnetometry, x-ray absorption spectroscopy, and x-ray magnetic circular dichroism. We find a significant change of the electronic structure at the martensitic phase transition. The lift of degeneracies in Ni $3d$ related unoccupied electronic states in the tetragonally distorted phase leads to a characteristic change of the x-ray absorption spectra, confirming a theoretical prediction for a transition from $c=a$ to $c < a$. The structural change in the vicinity of T_{MST} leads to a maximum value for the Ni orbital moment in this temperature region.

ACKNOWLEDGMENTS

The authors are grateful for financial support of the Deutsche Forschungsgemeinschaft (Ja821/3-1 within SPP1239

and EL-172/12-2). M.K. and H.J.E. thank S. Cramm for support at BESSY. G.J. thanks S. Roth from Institut für Werkstoffforschung, Dresden, for providing material for the sputtering target.

-
- ¹K. Ullakko, J. K. Huang, C. Kantner, R. C. OHandley, and V. V. Kokorin, *Appl. Phys. Lett.* **69**, 1966 (1996).
- ²A. Sozinov, A. A. Likhachev, N. Lanska, and K. Ullakko, *Appl. Phys. Lett.* **80**, 1746 (2002).
- ³O. Söderberg, Y. Ge, A. Sozinov, S.-P. Hannula, and V. K. Lindroos, *Smart Mater. Struct.* **14**, S223 (2005).
- ⁴P. J. Webster, K. R. A. Ziebeck, S. L. Town, and M. S. Peak, *Philos. Mag. B* **49**, 295 (1984).
- ⁵P. J. Brown, J. Crangle, T. Kanomata, M. Matsumoto, K.-U. Neumann, B. Ouladdiaf, and K. R. A. Ziebeck, *J. Phys.: Condens. Matter* **14**, 10159 (2002).
- ⁶V. V. Martynov and V. V. Kokorin, *J. Phys. III* **2**, 739 (1992).
- ⁷J. Pons, R. Santamaria, V. A. Chernenko, and E. Cesari, *J. Appl. Phys.* **97**, 083516 (2005).
- ⁸V. V. Khovailo, V. Novosad, T. Takagi, D. A. Filippov, R. Z. Levitin, and A. N. Vasilev, *Phys. Rev. B* **70**, 174413 (2004).
- ⁹A. T. Zayak, P. Entel, J. Enkovaara, and R. M. Nieminen, *J. Phys.: Condens. Matter* **15**, 159 (2003).
- ¹⁰S. R. Barman, S. Banik, and A. Chakrabarti, *Phys. Rev. B* **72**, 184410 (2005).
- ¹¹A. Ayuela, J. Enkovaara, and R. M. Nieminen, *J. Phys.: Condens. Matter* **14**, 5325 (2002).
- ¹²M. Lezaic, Ph. Mavropoulos, J. Enkovaara, G. Bihlmayer, and S. Blügel, *Phys. Rev. Lett.* **97**, 026404 (2006).
- ¹³Ch. Hordequin, E. Lelievre-Berna, and J. Pierre, *Physica B* **234-236**, 602 (1997).
- ¹⁴G. Jakob and H. J. Elmers, *J. Magn. Magn. Mater.* **310**, 2779 (2007).
- ¹⁵H. Schneider, G. Jakob, M. Kallmayer, H. J. Elmers, M. Cinchetti, B. Balke, S. Wurmehl, C. Felser, M. Aeschlimann, and H. Adrian, *Phys. Rev. B* **74**, 174426 (2006).
- ¹⁶M. Kallmayer, H. Schneider, G. Jakob, H. J. Elmers, B. Balke, and S. Cramm, *J. Phys. D* **40**, 1552 (2007).
- ¹⁷M. Kallmayer, H. Schneider, G. Jakob, H. J. Elmers, K. Kroth, H. Kandpal, U. Stumm, and C. Cramm, *Appl. Phys. Lett.* **88**, 072506 (2006).
- ¹⁸G. Jakob, F. Casper, V. Beaumont, S. Falk, N. Auth, H.-J. Elmers, C. Felser, and H. Adrian, *J. Magn. Magn. Mater.* **290-291**, 1104 (2005).
- ¹⁹B. T. Thole, P. Carra, F. Sette, and G. van der Laan, *Phys. Rev. Lett.* **68**, 1943 (1992).
- ²⁰G. van der Laan and I. W. Kirkman, *J. Phys.: Condens. Matter* **4**, 4189 (1992).
- ²¹Here, we choose the tetragonal notation $a=b \neq c$ and accordingly the cubic (220) reflection of the austenite is renamed to (202) in the martensite.